

SCIENTIFIC REPORTS

OPEN

NOX2 amplifies acetaldehyde-mediated cardiomyocyte mitochondrial dysfunction in alcoholic cardiomyopathy

Moritz Brandt^{1,2}, Venkata Garlapati², Matthias Oelze¹, Efthymios Sotiriou¹, Maike Knorr^{1,2}, Swenja Kröller-Schön¹, Sabine Kossmann¹, Tanja Schönfelder², Henning Morawietz⁴, Eberhard Schulz^{1,3}, Heinz-Peter Schultheiss⁵, Andreas Daiber^{1,3}, Thomas Münzel^{1,2,3} & Philip Wenzel^{1,2,3}

Alcoholic cardiomyopathy (ACM) resulting from excess alcohol consumption is an important cause of heart failure (HF). Although it is assumed that the cardiotoxicity of the ethanol (EtOH)-metabolite acetaldehyde (ACA) is central for its development and progression, the exact mechanisms remain obscure. Murine cardiomyocytes (CMs) exposed to ACA or EtOH showed increased superoxide ($O_2^{\bullet-}$) levels and decreased mitochondrial polarization, both being normalized by NADPH oxidase (NOX) inhibition. C57BL/6 mice and mice deficient for the ACA-degrading enzyme mitochondrial aldehyde dehydrogenase (ALDH-2^{-/-}) were fed a 2% EtOH diet for 5 weeks creating an ACA-overload. 2% EtOH-fed ALDH-2^{-/-} mice exhibited a decreased cardiac function, increased heart-to-body and lung-to-body weight ratios, increased cardiac levels of the lipid peroxidation product malondialdehyde (MDA) as well as increased NOX activity and NOX2/glycoprotein 91^{phox} (NOX2/gp91^{phox}) subunit expression compared to 2% EtOH-fed C57BL/6 mice. Echocardiography revealed that ALDH-2^{-/-}/gp91^{phox} mice were protected from ACA-overload-induced HF after 5 weeks of 2% EtOH-diet, demonstrating that NOX2-derived $O_2^{\bullet-}$ contributes to the development of ACM. Translated to human pathophysiology, we found increased gp91^{phox} expression in endomyocardial biopsies of ACM patients. In conclusion, ACM is promoted by ACA-driven mitochondrial dysfunction and can be improved by ablation of NOX2/gp91^{phox}. NOX2/gp91^{phox} therefore might be a potential pharmacological target to treat ACM.

Heart failure (HF) is a major public health problem with a prevalence of more than 23 million worldwide. Alcoholic cardiomyopathy (ACM) is a major contributor to the emerging epidemic of HF, accounting for about 3.8% of all cardiomyopathy cases¹ and 21–36% of nonischemic-dilated cardiomyopathy cases^{2,3}. ACM is characterized by an increase in left ventricular mass, dilation of the ventricles, wall thinning and ventricular dysfunction, with all these changes present in the absence of any other cause of intrinsic or extrinsic cardiomyopathy¹. Arrhythmias and electrocardiographic abnormalities may also be present in ACM patients with hemodynamically relevant alcohol-induced sinus bradycardia leading to recurrent syncope as the most significant bradyarrhythmia².

The amount and duration of per day consumption of ethanol (EtOH) sufficient to cause structural and functional myocardial alterations has been reported to start at as little as 80 g per day over 5 years^{1,4}; a finding that has recently been paralleled by a large meta-analysis, which saw a lack of protective associations among most age-specific and sex-specific alcohol use categories compared with non-alcohol consumers and thereby

¹Cardiology 1, Center for Cardiology, University Medical Center Mainz, Langenbeckstr. 1, 55131 Mainz, Germany.

²Center for Thrombosis and Hemostasis Mainz, University Medical Center Mainz, Langenbeckstr. 1, 55131 Mainz, Germany. ³German Center for Cardiovascular Research (DZHK), partner site Rhine Main, University Medical Center Mainz, Langenbeckstr. 1, 55131 Mainz, Germany. ⁴Division of Vascular Endothelium and Microcirculation, Department of Medicine III, University Hospital Carl Gustav Carus, Technische Universität Dresden, Fetscherstr. 74, 01307 Dresden, Germany. ⁵Institut für kardiologische Diagnostik und Therapie, Moltkestrasse 31, 12203 Berlin, Germany. Correspondence and requests for materials should be addressed to P.W. (email: wenzelp@uni-mainz.de)

challenged the long standing dogma of a protective effect of moderate alcohol consumption on cardiovascular diseases⁵.

Acetaldehyde (ACA) is considered the main culprit in the pathogenesis of ACM due to its high biochemical reactivity⁶ and its ability to concentrate in the myocardium⁷. Cytosolic alcohol dehydrogenase (ADH) forms ACA via partial oxidation of EtOH, while ACA is further oxidized to acetate by the mitochondrial aldehyde dehydrogenase (ALDH-2). Higher levels of ACA in drinkers with a genetic variation resulting in an overactive ADH (ADH 1C*1) were shown to be associated with an increased risk of several alcohol-related cancers⁸. In a mouse model of chronic alcohol administration, increased myocardial levels of ACA accelerated the development of cardiomyopathy in cardiomyocyte-specific ADH-overexpressing mice compared to control mice^{9–11}. Of note, even short-term exposure of CMs to ACA was sufficient to compromise cellular function in these cells⁶. Vice versa, EtOH severely compromised myocardial and cardiomyocyte function in wild-type FVB mice, whereas overexpression of ALDH-2 in transgenic mice abolished the detrimental effects of the acute¹² and chronic EtOH exposure¹³. These observations are also in good accordance with more recent findings that ALDH-2 is a cardio-protective enzyme that confers protection from ischemic damage during myocardial infarction and a significant decrease in the infarct area^{14,15}.

Similar to the overactive ADH 1C*1-isoform, the ALDH-2 mutant allele (ALDH-2*2) with a gene product that has no or very low ACA-oxidizing capacity¹⁶ leads to the accumulation of ACA. After alcohol consumption, carriers of this mutant allele experience symptoms caused by increased ACA often associated with the flushing syndrome¹⁷. It remains elusive, however, whether the cardiotoxicity of EtOH and ACA additionally involves reactive oxygen species (ROS). Interestingly, EtOH and ACA-induced mitochondrial O₂^{•-} production in mice with cardiac-specific overexpression of ADH resulted in activation of the mitochondrial death pathway and myocardial apoptosis¹⁰. Furthermore, EtOH metabolism itself can be a source of O₂^{•-}. In addition to ADH and ALDH-2, the cytochrome P450 (CYP) oxidase 2E1 is involved in EtOH metabolism¹⁸. Due to its induction by EtOH¹⁹, its importance might increase under conditions of chronic EtOH uptake. EtOH oxidation to ACA by CYP 2E1 involves the generation of hydroxyl radicals via the Fenton/Haber-Weiss reaction²⁰. However, ROS-generating enzymes like NOXs, specifically NOX2, activated by ACA via a transcriptional process might even outweigh the direct ROS production from EtOH breakdown²¹. This hypothesis of NOX as a factor in EtOH/ACA toxicity coincides with a large body of evidence that NOXs are involved in the pathogenesis of HF^{22,23}. NOX2 has been shown to drive HF as it contributes to cardiomyocyte hypertrophy, apoptosis and interstitial fibrosis^{24,25}. Hence, we investigated the role of myocardial ROS production and NOX function in the pathogenesis of ACM by inducing ACA-overload in EtOH fed ALDH-2^{-/-} mice and by generating ALDH-2^{-/-}/gp91^{phox-/-} mice.

Results

ACA-toxicity leads to decompensated HF with cardiomegaly, pulmonary edema and cardiac fibrosis in ALDH-2^{-/-} mice. When fed a 2% EtOH-Lieber-deCarli diet (EtOH diet) for 5 weeks (for protocol see Fig. 1A), ALDH-2^{-/-} mice had increased heart-to-body weight and lung-to-body weight ratios compared to ALDH-2^{-/-} mice fed the control diet or compared to C57BL/6 mice fed either diet (Fig. 1B,C), indicative of the onset of cardiac enlargement and pulmonary congestion in these animals.

Staining of cardiac sections with Picro-Sirius red yielded an intensive staining pattern throughout the entire myocardium in ALDH-2^{-/-} mice fed the 2% EtOH diet, which was not visible in ALDH-2^{-/-} mice fed the control diet or C57BL/6 mice fed either diet, pointing towards an increased collagen deposition as part of a fibrosis in the myocardium of these animals (Fig. 1D).

These findings reveal that in ALDH2^{-/-} mice, a 2% EtOH-Lieber-deCarli diet results in a HF phenotype with cardiomegaly, pulmonary edema and cardiac fibrosis.

NOX predominantly contributes to the ROS-associated myocardial damage in a mouse model of ACA toxicity. In order to investigate the underlying mechanism responsible for the HF phenotype resulting from the ACA-overload, we measured malondialdehyde (MDA) levels in tissue homogenates from ALDH-2^{-/-} mice and C57BL/6 mice (subjected to both diets) by dot-blot analysis. The myocardial MDA levels in EtOH-fed ALDH-2^{-/-} mice were the highest among all organs and significantly higher than the corresponding levels in EtOH-fed C57BL/6 animals and control-fed ALDH-2^{-/-} mice (Fig. 2A,B).

Cardiac membrane fractions from ALDH-2^{-/-} mice fed the EtOH diet produced a significantly higher O₂^{•-} signal than fractions from control-fed ALDH-2^{-/-} mice or from C57BL/6 mice fed either diet. Importantly, co-incubation with the NOX inhibitor diphenyleneiodonium (DPI) almost normalized the significantly increased chemiluminescence signal in myocardial membrane fractions from EtOH-fed ALDH-2^{-/-} mice (Fig. 2C).

Western blot analysis revealed a strong trend for increased expression of the NOX isoform NOX2 activator subunit p67^{phox} (p = 0.0539 vs. ALDH-2^{-/-} fed a control diet) and a significantly increased expression of the ubiquitously distributed NOX1 and NOX2 activator of the Rho-family, the GTPase Rac1 (Fig. 2D–F) in myocardial membrane fractions from EtOH-fed ALDH-2^{-/-} mice compared to control-fed ALDH-2^{-/-} mice or to C57BL/6 mice fed either diet.

Taken together, these findings point towards ROS mediated myocardial damage underlying the HF phenotype with cardiomegaly and cardiac fibrosis, and further points towards NOXs as major contributors to the detrimental ROS burden in our animal model of ACA toxicity.

Exposure of isolated CMs to EtOH or ACA induces upregulation NOX2 subunits and NOX2 activator proteins of the Rho family. To further investigate the effects of EtOH and ACA on the CM phenotype and to identify the NOX isoform responsible for the detrimental ROS burden in ACM, purified murine adult CMs were cultured in media containing EtOH or ACA (each 100 μM, equivalent to a blood concentration of 0.6% w/w) (for the protocol see Fig. 3A).

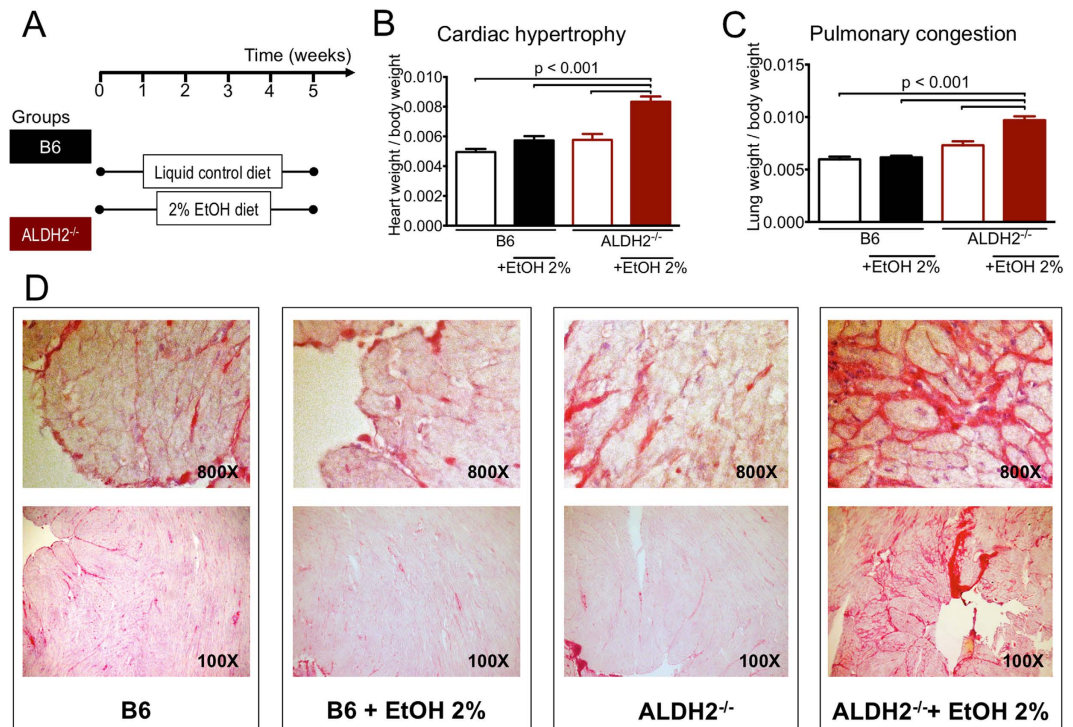


Figure 1. ACA-overload leads to cardiac enlargement myocardial fibrosis. (A) Scheme depicting the treatment of C57BL/6 and ALDH-2^{-/-} mice with 2% EtOH diet and liquid control diet. (B) Heart weight/body weight-ratios and (C) Lung weight/body weight-ratios in C57BL/6 and ALDH-2^{-/-} animals fed a 2% EtOH diet vs. liquid control diet. Data are presented as the mean \pm SEM from $n = 12-14$ animals per group. (D) Myocardial sections stained with Sirius-red from C57BL/6 and ALDH-2^{-/-} animals fed a 2% EtOH diet vs. liquid control diet.

The mRNA-expression of NOX2/gp91^{phox} and the NOX2 subunit p22^{phox} (a critical factor for stability and interaction of NOX2/gp91^{phox} and its cytosolic subunits) were significantly increased in CMs in the presence of ACA (Fig. 3B), while the expression of NOX activator Rac1 and the cytosolic subunit p47^{phox}, which is crucial for NOX2 activation²⁶, was significantly increased after culture in the presence of EtOH (Figs 3C and S3). Interestingly, the cell cycle regulator protein cell division cycle 42 (CDC42), which has been shown to mediate the NOX2-activation responsible for oxidative damage induced by arsenic in endothelial cells²⁷ and by ethanol in neurons²⁸, was significantly upregulated on the mRNA level in the presence of EtOH (Fig. 3C). Of note, the level of NOX4 mRNA did not change significantly in the presence of EtOH (Fig. S3).

As observed in brightfield phase contrast microscopy of live CMs, the detrimental effects of ACA were observable after culture for 18 h: While control-cultured CMs remained in the typical rod-shape, which enables CM function in the heart with clear boundaries and crisp sarcomeric structure at high magnification, ACA-cultured CMs degenerated to a round “meatball” shape indicating a terminal hypercontraction or exhibited cell blebbing and a total loss of the sarcomeric ultrastructure. Further addition of apocynin improved CM morphology and maintained rod-shape and intact ultrastructure (Fig. 3D).

Taken together, these findings reveal that the significantly increased ROS production underlying the HF phenotype is paralleled by significantly increased expression of NOX2 subunits and significantly increased expression of NOX2 activators in isolated CM cultured in the presence of EtOH or ACA.

Pharmacologic inhibition or genetic ablation of NOX reduces mitochondrial superoxide production in isolated CMs cultured in the presence of EtOH and ACA.

To assess whether upregulation of NOX2 subunits and NOX2 activators (Figs 2D–F and 3B,C) and increased NOX activity (Fig. 2C) after EtOH/ACA exposure is associated with increased production of mitochondrial ROS in CMs, as shown in endothelial cells²⁹, CMs cultured in the presence of EtOH or ACA with or without the NOX inhibitor apocynin (for the protocol see Fig. 4A) were subjected to automated live cell imaging and image quantification after loading with mitochondrially targeted dihydroethidium-based fluorescent dye MitoSOX (Fig. 4B). CMs cultured under control conditions exhibited low to moderate levels of mitochondrial ROS as long as they persisted in the typical rod-shape, thereby mimicking cells in the intact heart (Fig. 4B,C). Among the control CMs, only the few CMs that had transformed to the “meatball” shape indicating a terminal hyper-contraction displayed increased ROS levels. In contrast, CMs cultured in the presence of ACA showed significantly increased levels of mitochondrial ROS compared to controls. Co-treatment with the NOX inhibitor apocynin significantly reduced mitochondrial ROS levels in ACA-incubated CMs and, to a lesser extent, in EtOH-exposed CMs (Fig. 4B,C, empty arrows: cell in typical rod-shape, filled arrows: cells in terminal hypercontraction (“meatballs”).

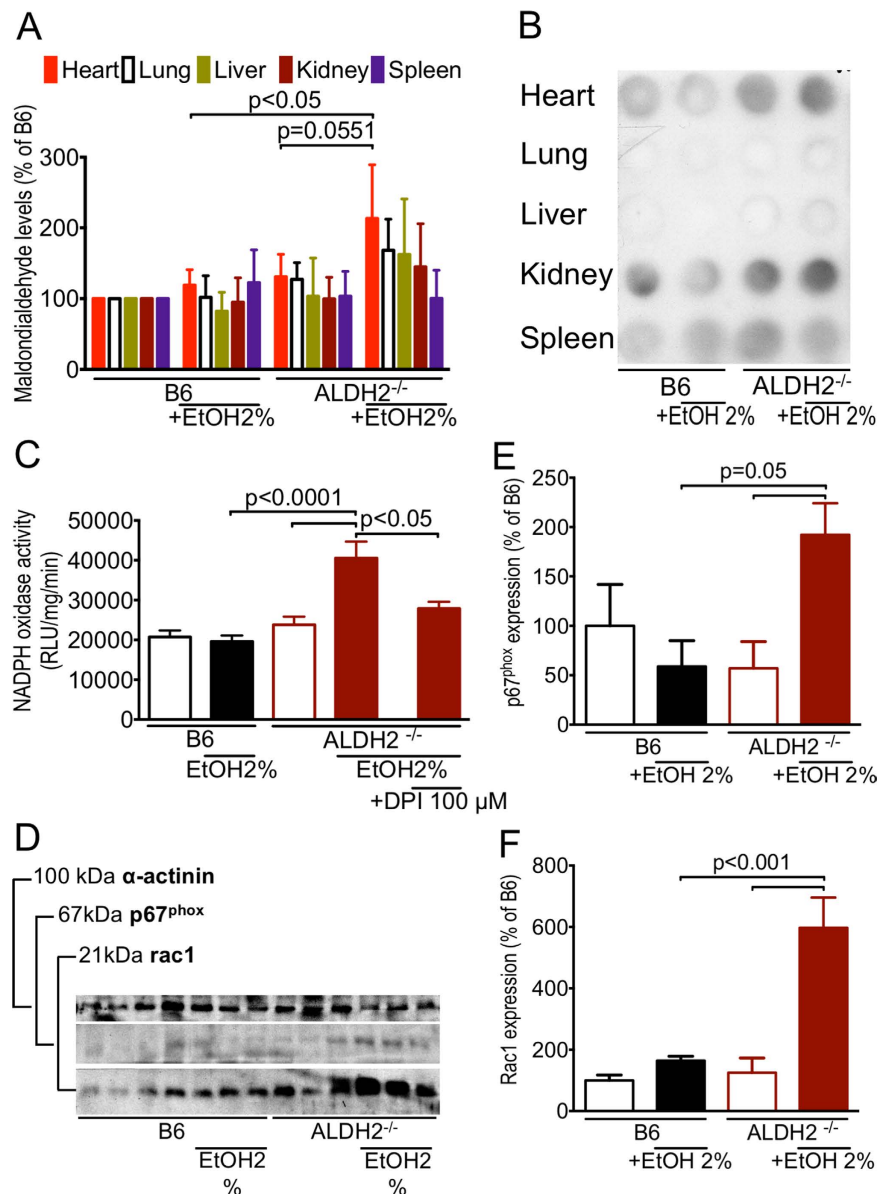


Figure 2. Increased myocardial ROS in ALDH2^{-/-} mice fed a 2% alcoholic diet. (A) Malondialdehyde levels in internal organs as determined by dot blot analysis of tissue homogenates. Data are expressed as mean \pm SEM from $n = 4$ per group. (B) Representative original dot blot; (C) NOX activity in myocardial membrane fractions determined by lucigenin-derived chemiluminescence. Data are presented as mean \pm SEM from 18–20 measurements of $n = 5$ animals per group. (D) Representative original Western blot. (E) p67^{phox} protein expression and (F) Rac1 protein expression determined by Western blot. Data presented as mean \pm SEM from $n = 3$ –4 animals per group.

MitoSOX, a mitochondrially targeted ROS sensitive fluorescent dye, allows for a quantitative assessment of mitochondrial oxidants within the complex context of live cells, which was required to elucidate the interplay of NOX2 and mitochondria^{29,30} in our setting of EtOH/ACA mediated CM dysfunction. However, some inaccuracy as to the exact species, source and location of ROS remains: MitoSOX (Mito-hydroethidine) has multiple oxidation products of which only 2-hydroxyethidium is specific for $O_2^{\bullet -}$. Also MitoSOX can lead to collapse of $\Delta\Psi_m$ with it or its oxidation products leaking into the cytosol³¹, thereby staining other cell compartments and it has a high affinity for polyanionic macromolecules such as mitochondrial as well as nuclear DNA^{32,33}. To partially compensate for this (1) we conducted a co-staining of MitoSOX with MitoTracker Green FM, which localizes to mitochondrial membranes irrespective of mitochondrial polarization, and (2) applied an orthogonal assay, the quantification of peroxiredoxin 3, a mitochondrial specific marker for oxidative stress by Western blot^{34,35}.

As visible in high power images, culture in the presence of ACA resulted in a ROS signal with an even areal distribution throughout the CMs, and which overlapped with the localization of mitochondria as indicated by areal green fluorescence to a large degree. Additional MitoSOX enhanced nuclear fluorescence resulted from the fragility of primary adult CMs with MitoSOX oxidation products leaking from the mitochondria and staining

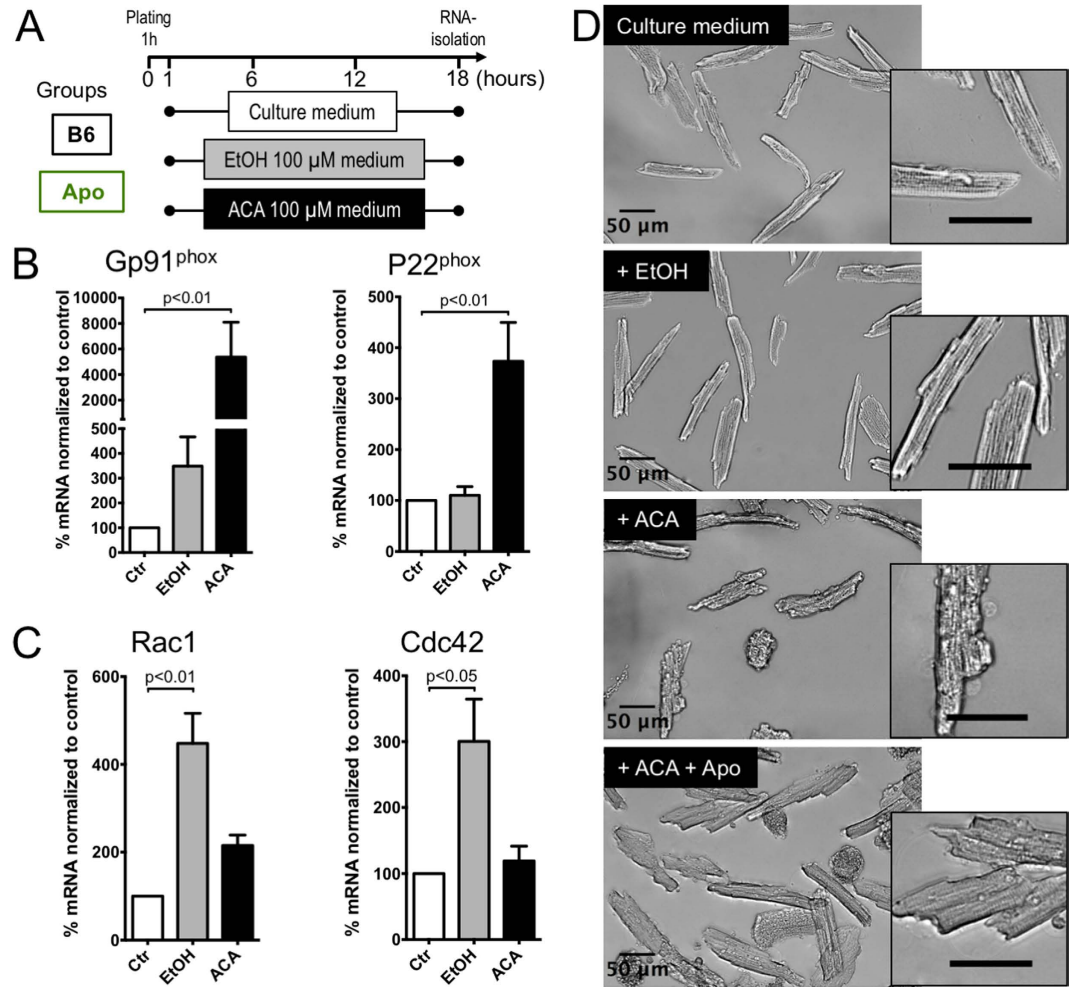


Figure 3. Exposure of isolated CMs to EtOH or ACA induces upregulation of NOX. (A) Scheme depicting incubation of isolated adult CMs with EtOH (100 μ M) or ACA (100 μ M). (B) Expression of NOX2 subunit gp91^{phox} and p22^{phox}. (C) Expression of Rac GTPase Rac1 and of the Rho-family GTP binding protein cell division cycle 42 (CDC42). (D) Brightfield images of live mouse adult CMs after incubation in media supplemented with EtOH or ACA with or without apocynin, the scale bars were kept at 50 μ M. (B,C) Data presented as the mean \pm SEM.

nuclear DNA due to their high affinity for polyanionic macromolecules. Co-treatment with apocynin resulted in an almost complete loss of the mitochondrial MitoSOX signal, underlining the role of NOX2 in the generation of mitochondrial ROS (Fig. 4C).

These data show that pharmacologic inhibition of NOX significantly lowers cytosolic and mitochondrial levels, which were significantly increased after exposure to ACA. Importantly, while the decrease in cytosolic ROS can be explained by a reduced $O_2^{\bullet-}$ release from NOXs, the reduced levels of mitochondrial ROS hint towards an interplay of NOX activation and mitochondrial ROS production in CMs in our setting of EtOH induced HF/ACA-overload, a mechanism that has been described in angiotensin II-induced oxidative stress^{29,30}.

Peroxiredoxin 3 (Prx 3, mitochondrial matrix peroxiredoxin) is a mitochondrially located member of the peroxiredoxins, an ubiquitous family of antioxidant enzymes that are involved in cell signaling by regulating H_2O_2 levels³⁶. Prx 3 exists in a monomeric, reduced thiol form and a dimeric, oxidized disulfide form, while the ratio of reduced to oxidized form serves as a specific marker for mitochondrial oxidative stress as shown by others and by our group^{34,35}.

Compared to control cultured CMs, CMs cultured in the presence of EtOH or ACA exhibited a gradual reduction of the Prx 3 monomer/dimer ratio, while the ratio in ACA-exposed CMs was significantly reduced as determined by non-reducing Western blot. Of note, CMs isolated from ALDH2^{-/-} exposed to EtOH revealed a monomer/dimer ratio comparable to B6 CMs exposed to equimolar doses of ACA, while the additional lack of gp91^{phox} in CMs isolated from ALDH2^{-/-} gp91^{phox}^{-/-} double knockout mice significantly increased the monomer/dimer as compared to EtOH treated ALDH2^{-/-} CMs back to the level of control treated B6 CMs (Fig. 4D,E).

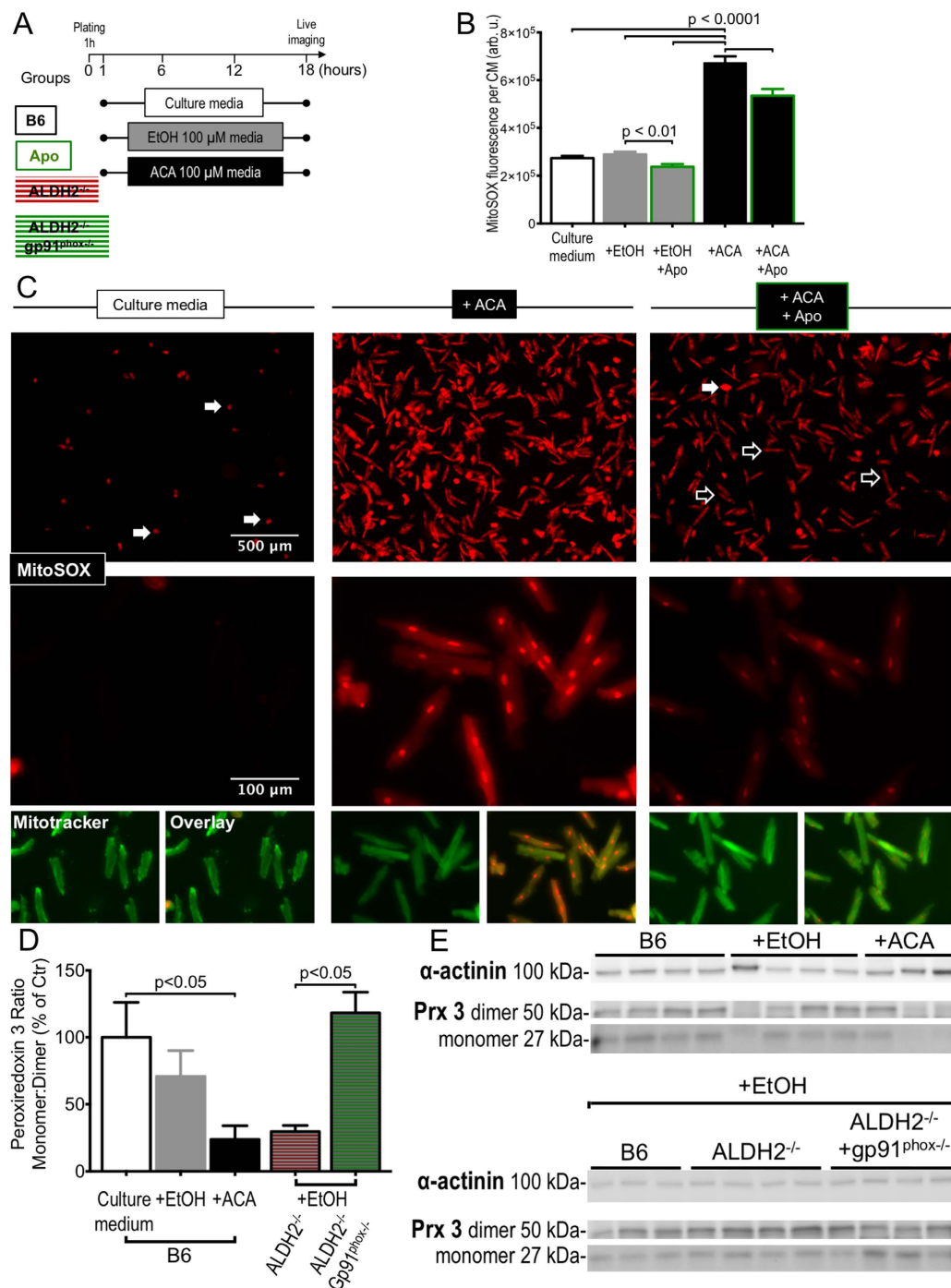


Figure 4. Pharmacologic inhibition or genetic ablation of NOX reduces mitochondrial superoxide production in isolated CMs cultured in the presence of EtOH and ACA. (A) Scheme depicting incubation and imaging of isolated adult CMs from B6, ALDH2^{-/-} or ALDH2^{-/-}/gp91^{phox-/-} mice with apocynin (300 μM), EtOH (100 μM) or ACA (100 μM). (B) MitoSOX-enhanced fluorescence per CMs. Quantification of 205–931 CMs on 6–12 independent low power fields per group. (C) Representative fluorescence images of CMs loaded with MitoSOX after culture for 18h in control media (leftmost column) in the presence of ACA 100 μM (middle column) and in the presence of ACA (100 μM) together with the NOX inhibitor apocynin (300 μM) rightmost column. (D) Peroxiredoxin 3 ratio monomer/dimer determined by Western blot under non-reducing, denaturing conditions in n = 4–7 independent samples per group. (E) Representative original Western blots.

These results further provide an independent support of our hypothesis of increased mitochondrial oxidative stress upon CM exposure to EtOH and especially ACA (directly and indirectly by the lack of ALDH-2) and further stress the role of NOX2 in the induction of mitochondrial ROS.

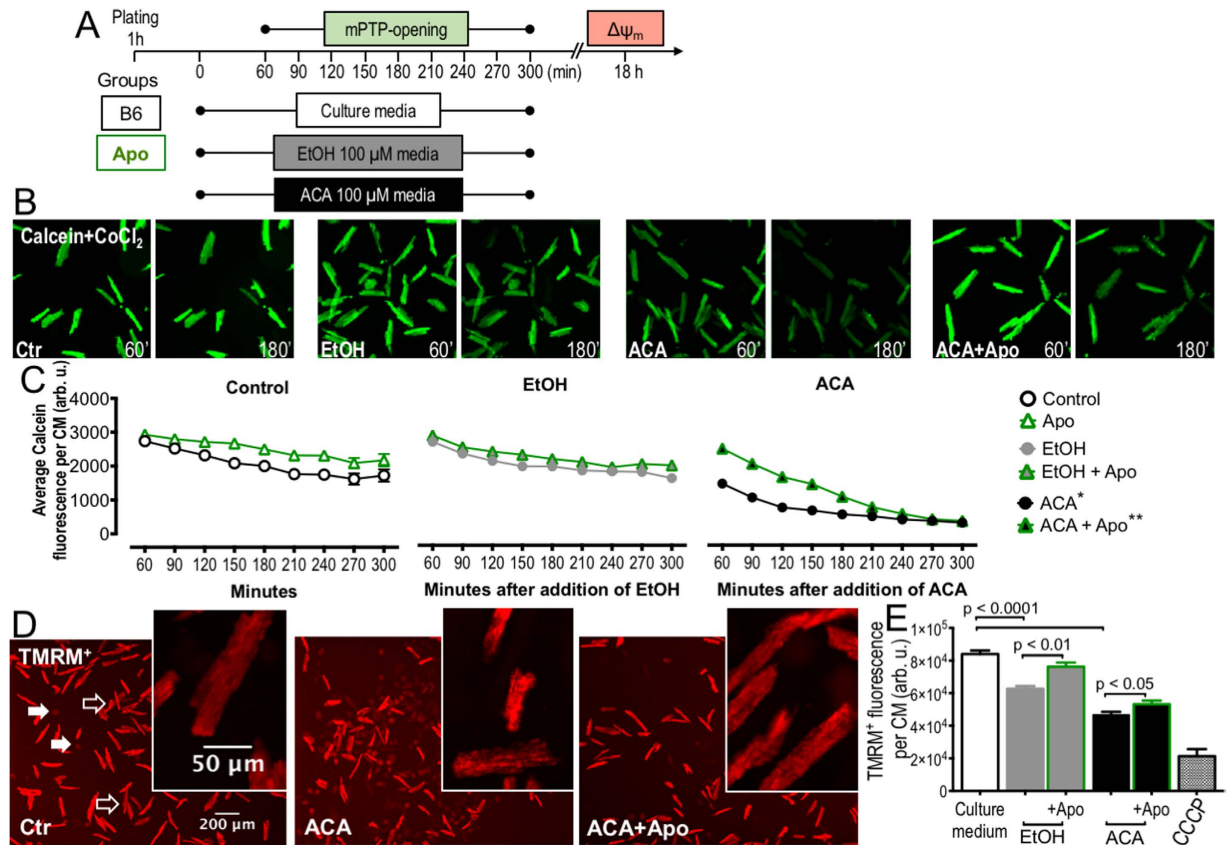


Figure 5. Inhibition of NOX prevents opening of the mitochondrial permeability transition pore (mPTP) and maintains mitochondrial polarization ($\Delta\Psi_m$) in isolated CMs exposed to EtOH/ACA. (A) Scheme depicting incubation and imaging of isolated adult CMs with EtOH (100 μ M) or ACA (100 μ M). (B) CM fluorescence after loading with calcein/CoCl₂ and after incubation with EtOH or ACA and ACA+Apo, representative images. (C) Quantification of average calcein/CoCl₂ derived fluorescence per CM, quantification Calcein/CoCl₂ enhanced fluorescence of 100 CMs in 6–12 low power fields per group, * $p < 0.01$ vs Control, ** $p < 0.01$ vs ACA. (D) CM fluorescence after loading with the voltage-sensitive fluorescent probe TMRM⁺ and after incubation with ACA and ACA+Apo, representative images. (E) Quantification of TMRM⁺-enhanced fluorescence of 416–887 CMs on 6–12 independent low power fields per group, black bar “+CCCP” depicts CM background fluorescence after mitochondrial depolarization with the ionophore/uncoupler carbonyl cyanide *m*-chlorophenyl hydrazone (CCCP) (Fig. S2). (C,E) Data presented as the mean \pm SEM.

Inhibition of NOX attenuates increased mitochondrial ROS formation and improves impaired $\Delta\Psi_m$ in isolated CMs exposed to EtOH/ACA. In order to test how our results of increased levels of EtOH/ACA induced mitochondrial oxidative stress correlate with mitochondrial integrity, we aimed to assess two parameters of mitochondrial function: opening of the mitochondrial permeability transition pore (mPTP) and mitochondrial polarisation ($\Delta\Psi_m$).

To assess mPTP-opening, CMs cultured in the presence of EtOH or ACA with/without apocynin were loaded with the fluorescent dye calcein-AM, which, after deesterification, is not able to cross the intact inner mitochondrial membrane (IMM) and is trapped in the mitochondria. Further addition of CoCl₂ quenches only the cytosolic and nuclear fluorescence, as CoCl₂ cannot enter mitochondria across the IMM (for the protocol see Fig. 5A). While calcein/CoCl₂ enhanced mitochondrial fluorescence remained stable in control cultured CMs, ACA-cultured CMs exhibited a significant loss of calcein/CoCl₂ enhanced mitochondrial fluorescence, suggesting a relevant mPTP-opening in these cells. Co-incubation of ACA-exposed CMs with apocynin was able to delay the loss of fluorescence and temporarily prevent mPTP-opening. EtOH-exposed CMs only revealed little loss of fluorescence as compared to control cultured CMs. Interestingly, co-incubation with apocynin seemed to prevent mPTP opening in all three groups, although the effect was most eminent in ACA-cultured CMs (Fig. 5B,C).

To further assess mitochondrial polarization, which represents a key feature of healthy mitochondria and a prerequisite for ATP production by complex V, CMs cultured in the presence of EtOH or ACA with or without apocynin were loaded with the membrane-permeable, voltage-sensitive fluorescent probe TMRM⁺. The majority of control-incubated CMs was rod-shaped and showed bright TMRM⁺-dependent fluorescence, indicating active, polarized mitochondria (Fig. 5D empty arrows), while higher magnification revealed a homogenous distribution of active mitochondria throughout the CM. Only a few CMs with dim fluorescence, indicative of

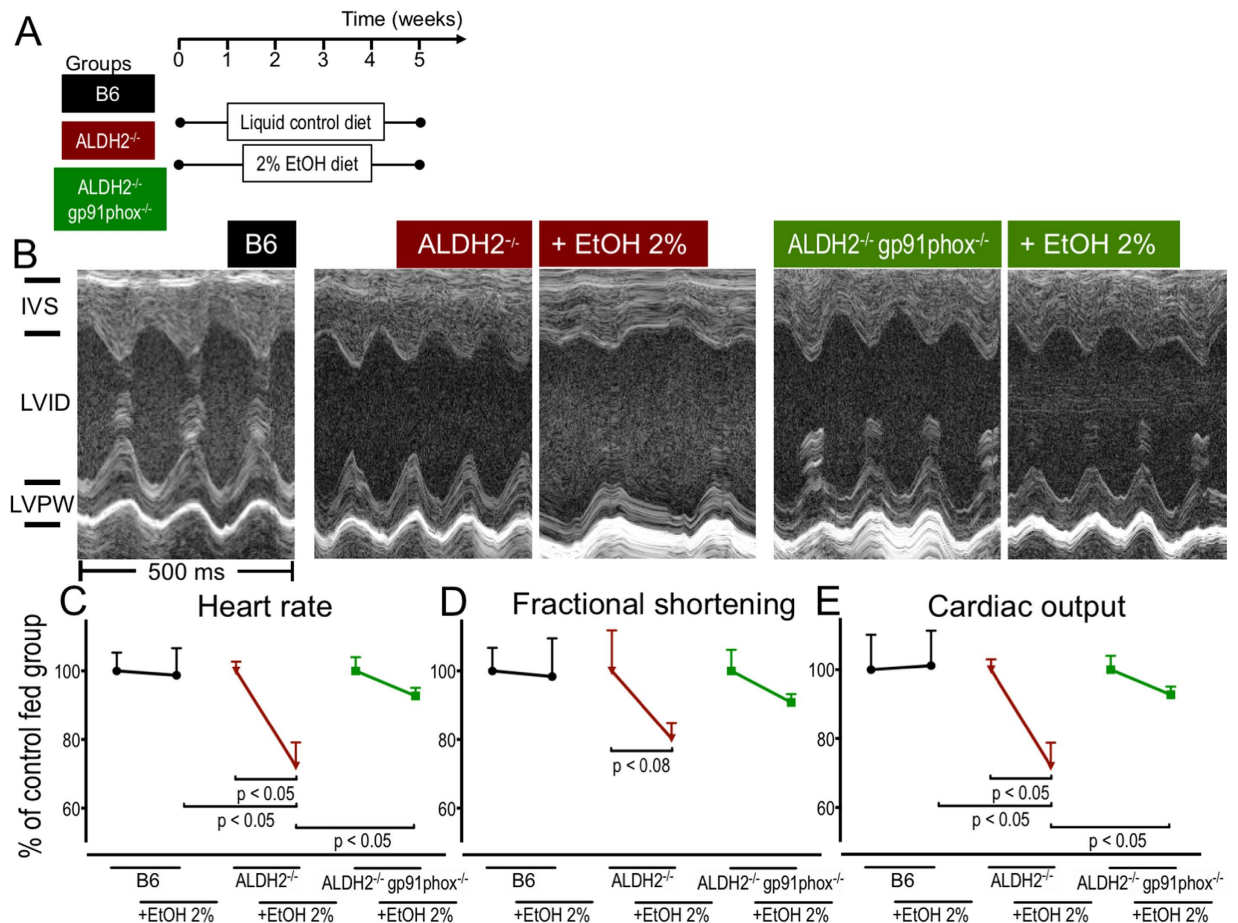


Figure 6. Lack of NOX2/gp91^{phox} protects from alcoholic cardiomyopathy induced by ACA-overload.

(A) Scheme depicting the treatment of C57BL/6, ALDH2^{-/-}, and ALDH2^{-/-}/gp91^{phox} mice with 2% EtOH diet and liquid control diet. (B) Representative M-mode tracings. (C) Heart rate, (D) Fractional shortening and (E) Cardiac output. Data are presented as mean ± SEM from n = 5–12 animals per group and normalized to the respective genotype fed the liquid control diet.

mostly depolarized mitochondria, were visible. Importantly, dim fluorescence and depolarized mitochondria coincided with the terminal hypercontraction, in accordance with the increased ROS levels (Figs 4C and 5D filled arrows).

Both EtOH- and ACA-cultured CMs showed a significantly reduced TMRM⁺-dependent fluorescence, indicating an overall reduced mitochondrial activity, while at the subcellular level, high magnification revealed a non-homogenously distributed mitochondrial activity. Here, active to hyperpolarized mitochondria were observed adjacent to dark areas devoid of active mitochondria. Many CMs had deteriorated to hypercontraction. Of note, the impact of ACA on mitochondrial activity was more detrimental than EtOH in accordance with the higher ROS levels in these cells (Figs 4C and 5D,E).

Co-treatment with apocynin improved overall mitochondrial activity in both ACA- and EtOH-incubated CMs and reduced the number of hypercontractile CMs. At the subcellular level, it restored the homogenous distribution of active mitochondria (Fig. 5D,E).

The cardinal function of cardiac mitochondria is to generate chemical energy in form of ATP to enable the actin/myosin interaction underlying CM contraction. Our experiments underline the impact of EtOH- and especially ACA-induced, NOX2-mediated mitochondrial ROS on two key parameters of mitochondrial function, namely mPTP-opening and $\Delta\Psi_m$, thereby establishing the link between ACA-overload and CM dysfunction.

Lack of NOX2/gp91^{phox} protects from HF in a model of ACA-overload. In order to test whether our finding of EtOH/ACA induced, NOX2 mediated increase of mitochondrial ROS leading to impaired mitochondrial and thus impaired CM function, together with the beneficial effects of pharmacologic NOX inhibition or genetic NOX2 ablation *in vitro* could be reproduced *in vivo*, we crossbred ALDH2^{-/-} mice with mice null for the NOX isoform NOX2 (NOX subunit gp91^{phox}) resulting in the ALDH2^{-/-}/gp91^{phox} double knockout mice and subjected mice of all genotypes (C57BL/6, ALDH2^{-/-} and ALDH2^{-/-}/gp91^{phox} to EtOH vs. control diet (for the protocol see Fig. 6A).

While neither EtOH nor control diet had an effect on cardiac function in C57BL/6 mice, the EtOH diet had a dramatic impact on the cardiac function in ALDH2^{-/-} mice. Compared to control-fed ALDH2^{-/-} mice,

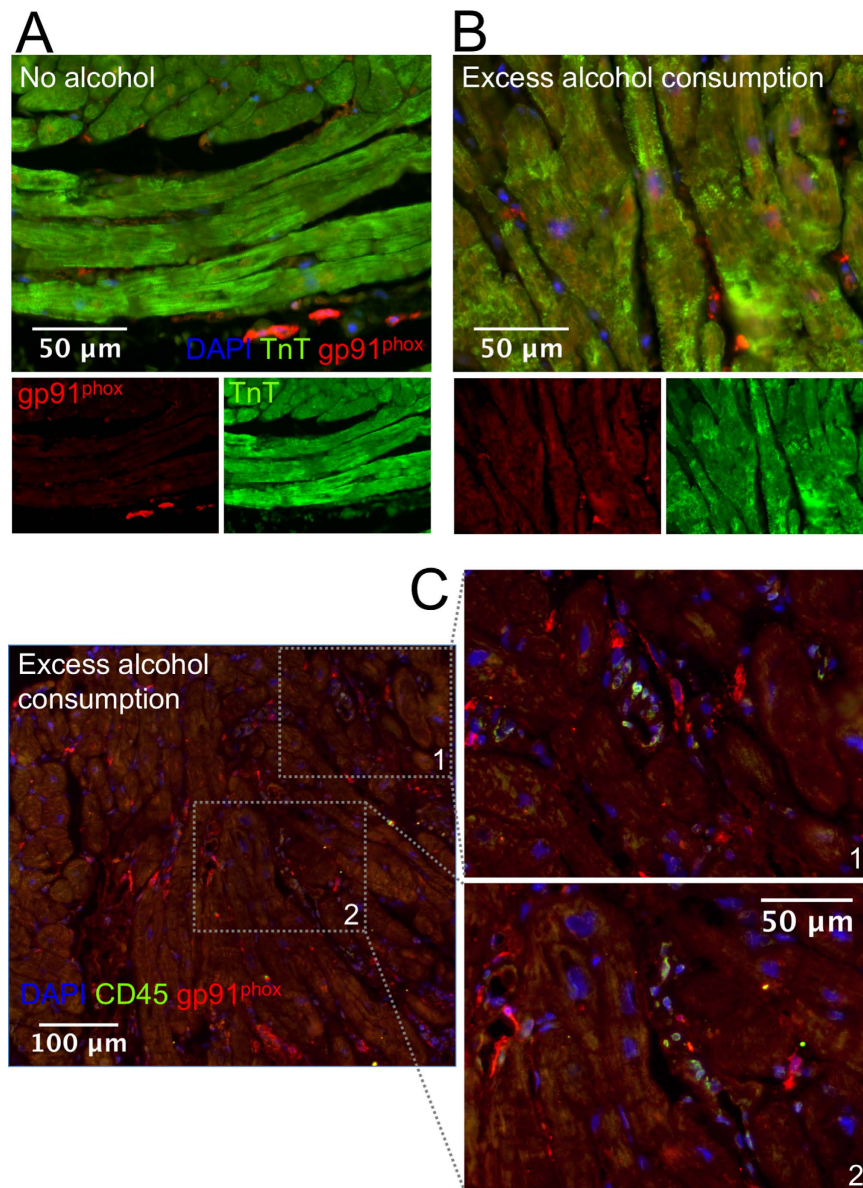


Figure 7. Increased NOX2/gp91^{phox} expression in CMs of HF patients with alcohol abuse. (A–C) Representative images from sections from human myocardial biopsies (red, gp91^{phox} staining; blue, DAPI-stained nuclei; A+B green, cardiac troponin T staining; C green, CD45). Excess alcohol consumption was defined as an uptake of EtOH exceeding 60 g per day.

EtOH-fed ALDH-2^{-/-} mice (for the protocol see Fig. 6A) showed a reduced fractional shortening and a significantly decreased heart rate resulting in a significantly impaired cardiac output (Fig. 6B–E). This was consistent with the histomorphometric alterations of cardiac enlargement, pulmonary congestion and increased myocardial fibrosis observed in these animals (Fig. 1B–D).

Additional knockout of NOX2/gp91^{phox} attenuated the detrimental effect of the EtOH diet. It improved fractional shortening and normalized heart rate, resulting in a significantly ameliorated cardiac output in ALDH-2^{-/-}/gp91^{phox}^{-/-} double knockout mice as compared to ALDH-2^{-/-} mice (Fig. 6B–E).

Cardiomyocyte expression of NOX2/gp91^{phox} is increased in patients with HF with reduced ejection fraction and a history of excess alcohol consumption.

In order to translate our findings to human pathophysiology, we examined patients suffering from HF with reduced ejection fraction who were admitted to our centre for diagnostic work-up. We investigated endomyocardial biopsy specimen taken routinely for diagnostic purposes according to current guidelines. We found a significant upregulation of NOX2/gp91^{phox} expression in CMs from patients with a history of excess alcohol consumption compared to matched controls (Fig. 7 and Table 1). In contrast, cardiac levels of amyloid, incident viral replication (EBV, HHV6, Enterovirus or Adenovirus) or burden of infiltrating CD3⁺ T-cells, Mac-1⁺ myeloid cells or LFA-1⁺ inflammatory cells were not different between groups.

	Dilated cardiomyopathy (DCM)-morphology, no history of alcohol consumption	Dilated cardiomyopathy (DCM)-morphology, with history of excess alcohol consumption	p-Value
N	7	7	
Age (y)	64.3 ± 3.37	62 ± 3.34	p = 0.3969
Histologic signs of acute or chronic inflammation	0/7	0/7	
History of excess alcohol consumption	0/7	7/7	
Left ventricular ejection fraction (%)	27.14 ± 1.71	24 ± 3.29	p = 0.7159
LVEDD (cm)	6.66 ± 0.43	6.30 ± 0.26	p = 0.625
Cardiomyocyte diameter (µm)	19.71 ± 1.51	26.83 ± 2.25	p = 0.0554
Amyloid	0/7	0/7	
Adenovirus-positive	0/7	0/7	
HHV6-positive	0/7	0/7	
EBV-positive	1/7	0/7	
Enterovirus (Coxsackie)-positive	0/7	0/7	
CD3 ⁺ cells/mm ²	3.41 ± 1.31	4.03 ± 2.56	p > 0.9999
Mac-1 ⁺ cells/mm ²	12.87 ± 2.16	19.98 ± 1.33	p = 0.0952
LFA-1 ⁺ cells/mm ²	10.52 ± 0.92	12.41 ± 4.07	p = 0.9683
gp91 ^{phox} -Expression	1.35 ± 0.06	1.70 ± 0.06*	p = 0.0079

Table 1. Increased NOX2/gp91^{phox} expression in CMs of HF patients with a history of excess alcohol consumption. Left ventricular ejection fraction and LVEDD were determined by echocardiography. Histologic and immunohistochemical analyses were performed at the Institute for Cardiac Diagnostics and Therapy (IKDT, Berlin). Gp91phox expression was quantified by digital image analyses after immunostaining. Data are presented as mean ± SEM. HHV6, human herpes virus 6, EBV, Epstein-Barr-virus; Mac-1, integrin $\alpha_M\beta_3$; LFA-1, lymphocyte function associated antigen 1. Excess alcohol consumption was defined as an uptake of EtOH exceeding 60 g per day.

To determine whether the increased myocardial NOX2 expression in our setting of excess alcohol consumption could be due to excessive leukocyte infiltration or due to increased expression of NOX2 by myocardial leukocytes, we conducted a co-staining of the investigated biopsies for NOX2/gp91^{phox} and the leukocyte marker CD45. Interestingly, in biopsies from both groups, the number of myocardial CD45⁺ cells were too low to render a significant contribution of these cells to the myocardial NOX2 expression probable (Fig. 7C).

Discussion

The onset of ACM correlates with a high daily level of alcohol consumption over an extended period of time¹. To our knowledge, this is the first study investigating the chronic effects of ACA-overload as a central event in the development of ACM using ALDH-2^{-/-} mice subjected to a long-term EtOH diet. Importantly, the animals displayed key characteristics of ACM¹, namely the HF phenotype with cardiomegaly and cardiac fibrosis leading to functional cardiac compromise including significant sinus bradycardia, reduced fractional shortening, a significantly reduced cardiac output and consecutive pulmonary congestion, all characteristics that have been described in the human disease phenotype, while these pathologic features were absent in control diet-fed ALDH-2^{-/-} mice and C57BL/6 mice fed the ethanol diet (Fig. 1B–D, Fig. 6B–E). Interestingly, myocardial fibrosis in EtOH-fed ALDH-2^{-/-} mice (Fig. 1D) as an important feature of HF is absent in most murine models of ACM³⁷.

We observed a greatly increased susceptibility in ALDH-2^{-/-} mice to EtOH toxicity, which emphasizes the role of ACA in the pathogenesis of ACM. In ALDH-2^{-/-} mice, the phenotype was already apparent after 5 weeks of 2% EtOH liquid diet compared to 14 weeks of 4% EtOH liquid diet in wild type mice reported in earlier studies¹³, while our pilot studies had revealed that ALDH-2^{-/-} mice died after 3 days of 6% EtOH and after 3 weeks of 4% EtOH Liber-diCarli diet feeding.

The ACM phenotype in EtOH-fed ALDH-2^{-/-} mice was accompanied by significantly increased myocardial MDA levels (Fig. 2A,B), which were strongly indicative of increased levels of myocardial ROS as the central phenomenon of ACM in EtOH-fed ALDH-2^{-/-} mice in line with previous studies^{6,10}. In support of the higher susceptibility of ALDH-2^{-/-} mice for mitochondrial ROS formation, we had previously shown that nitroglycerin treatment results in higher mitochondrial oxidative stress burden in ALDH-2^{-/-} mice as compared to controls³⁸. Importantly, the MDA levels correlated with significantly increased NOX activity in myocardial membranous fractions from EtOH-fed ALDH-2 mice compared to control-fed ALDH-2^{-/-} or C57BL/6 mice fed the EtOH-diet (Fig. 2C).

As it is known that ROS play a central role in the pathogenesis of HF, the specific ROS effects depend upon the location, concentration, duration, nature and source of the reactive species. NOX enzymes are capable of ROS production in a tightly regulated fashion. Different NOX isoforms are present in the cardiovascular system, of which NOX2 and NOX4 are the most abundantly expressed isoforms in CMs²².

NOX4 seems to comprise cardioprotective abilities, as it was found to protect against chronic pressure overload by counteracting the associated ROS through upregulation of antioxidant genes via Nrf2³⁹ and by increasing myocardial angiogenesis via induction of HIF-1 α ⁴⁰.

The role of NOX2 is more ambiguous: NOX2-derived $O_2^{\bullet-}$ mediates mechanotransduction and Ca^{2+} signalling in healthy CMs⁴¹ and in a few specific settings; similar to NOX4, it seems to prevent HF as by decreasing infarct size after preconditioning through improved Ca^{2+} handling in CMs⁴².

However, unlike NOX4, in most contexts NOX2 was also shown to aggravate HF: NOX-2 drives CM hypertrophy in response to stimulation with angiotensin II, noradrenaline, endothelin-1, aldosterone and mechanical stress after aortic constriction through adapter proteins and transcription factors (including Ras/Erk, ASK-1 and NF- κ B)²². NOX2 is further involved in CM apoptosis via activation of CaMKII⁴³. In myocardial fibrosis, NOX2 acts in concert with MMPs, PI3K γ and CTGF^{44–46}.

In line with these previous findings, with our results of significantly increased NOX activity in heart membrane fractions, increased expression of NOX2 activating subunit p67^{phox} and significantly increased expression of NOX2-activating protein Rac1 in myocardial membrane fractions (Fig. 2C–F) and increased expression of NOX2/gp91^{phox}, p22^{phox} (NOX2 subunit critical for correct assembly) and Rac1 after culture of isolated CMs in the presence of EtOH/ACA (Fig. 3B,C), we could corroborate previous evidence that NOX2 is upregulated in the development of ACM¹³, while NOX4, the only other NOX isoform expressed in CMs, appeared not to be involved (Fig. S3).

By studying isolated and purified CMs we were able to address the question whether NOX2 is just a bystander or a culprit that exacerbates the myocardial dysfunction in ACM.

Cultured CMs after exposure to ACA exhibited significantly increased levels of cytosolic, and in particular mitochondrial ROS as indicated by MitoSOX-enhanced fluorescence, which overlapped with mitochondrial specific staining to a large degree and as confirmed orthogonally by significant oxidation of the mitochondrial specific enzyme Prx 3^{34–36} in ACA-exposed CMs compared to control cultured CMs (Fig. 4B–E). The increased levels of mitochondrial ROS were paralleled by a significant mPTP-opening and significant reduction of $\Delta\Psi_m$, indicating a compromise of mitochondrial health and cellular function in CMs cultured in the presence of ACA (Fig. 5B–D). Pharmacologic NOX inhibition and genetic ablation of NOX2 significantly reduced mitochondrial ROS (Fig. 4B–E) and were able to significantly delay opening of the mPTP, partially restore $\Delta\Psi_m$ and thereby partially preserve CM mitochondrial function (Fig. 5B–D) and CM morphology (Fig. 3D). These findings hint towards a functional connection of NOX2-derived ROS and mitochondrial dysfunction.

Mitochondrial dysfunction in CMs is a hallmark of HF of different etiologies including ACM^{10,23}. In our setting, mitochondrial dysfunction mechanistically links excess ROS due to increased NOX2 activity to cardiomyopathy and provides an explanation of how ACA imposes its toxicity on CMs and impairs cardiac function. Using isolated and purified cells, we were able to observe that in CMs, NOX2, which is localized in the cytosol outside the mitochondria, can interfere with intra-mitochondrial processes, presumably using $O_2^{\bullet-}$ as a signalling molecule in accordance with studies that angiotensin II-induced mitochondrial dysfunction in endothelial cells was shown to be NOX-dependent, as both apocynin and p22^{phox} knockdown were able to preserve mitochondrial function^{29,30}. Similarly, chronic nitroglycerin treatment induced mitochondrial $O_2^{\bullet-}$ with subsequent NOX activation leading to the spatially separated phenomena of nitrate tolerance (depending on mitochondrial $O_2^{\bullet-}$ formation) and endothelial dysfunction (depending on NOX activation)⁴⁷. In this phenomenon, termed “the NOX-mitochondria crosstalk”, NOX2 derived ROS can trigger mitochondrial ROS formation in a protein kinase C, mitochondrial ATP-sensitive potassium channel (K_{ATP} channel) and loss of $\Delta\Psi_m$ dependent fashion as shown by others and our group^{29,47,48}.

The role of NOX2 in the pathogenesis of ACM was further supported by *in vivo* data from mice lacking NOX2/gp91^{phox} in addition to ALDH-2, as these mice were partially protected from the cardiotoxic effects of ACA-overload (Fig. 6).

Further, our findings that NOX2/gp91^{phox} is significantly higher expressed in CMs of individuals with HF and a history of chronic abuse of high amounts of alcohol (>60 g/d) indicate that our experimental findings in principle hold true in human ACM (Table 1, Fig. 7A,B).

While we provide evidence that ACA induces a NOX-2 mediated CM mitochondrial dysfunction in alcoholic cardiomyopathy, it remains to be established how excess ACA leads to increased NOX2 subunit expression and increased NOX activity. The cell cycle regulator protein Cdc42 could provide an explanation: This protein has been shown to mediate the NOX2 activation responsible for oxidative damage induced by EtOH in neurons²⁸ (and by arsenic in endothelial cells²⁷) and Cdc42 was upregulated in CMs after culture in the presence of EtOH in our hands (Fig. 3C).

Further, the NOX2 activator subunit p67^{phox}, which was upregulated in myocardial membrane fractions of EtOH-fed ALDH-2^{-/-} mice, is regulated by the transcription factors PU.1, IRF1 and ICSBP⁴⁹, two of these, PU.1 and IRF1, have been shown to be upregulated by EtOH^{50,51} representing a putative molecular mechanism of NOX2 activation in this context.

Finally, as a primary mechanism or in a vicious circle, after initial production of kindling $O_2^{\bullet-}$ -radicals by NOX2, ROS from dysfunctional mitochondria could trigger NOX2 activation in a mPTP-, protein kinase C- and tyrosine kinase cSrc-dependent fashion as recently shown, termed “the mitochondria-NADPH oxidase crosstalk”^{52,53}.

It remains to be established which ROS source provides the kindling radicals and which one serves as an amplifier of this initial oxidant formation resulting in a vicious circle. In conclusion, our data suggest that myocardial NOX2 in response to ACA overload is involved in the pathogenesis of ACM and interferes with the mitochondrial function in CMs. Pharmacologic inhibition of NOX2, mitochondrial ROS formation and/or mitochondrial permeability might present novel targets to prevent alcoholic cardiomyopathy *in vivo*.

Material and Methods

Animal model. All animal experiments were in accordance with the Declaration of Helsinki and National Institutes of Health guidelines. All experiments were approved by the Ethics Committee of the University Hospital Mainz and by the Institutional Animal Care and Use Committee (IACUC; Landesuntersuchungsamt

Rheinland-Pfalz, Koblenz, Germany). All mice were housed in a barrier facility (TARC, Translational Animal Research Center, University Medical Center Mainz), kept in filtertop cages with 2–5 mice per cage under specific pathogen-free (SPF) conditions. Male 6–8 weeks old C57BL/6, ALDH-2^{-/-} and ALDH-2^{-/-}/gp91^{phox}^{-/-} mice (both on C57BL/6 background) were age-matched and divided into 6 treatment groups comparing control-fed versus EtOH-fed groups of each genotype. The EtOH diet was a modified Lieber-deCarli liquid diet⁵⁴. The 2% EtOH-Lieber-deCarli diet consisted of 20 mL/L 100% EtOH, 61.4 g maltose dextrin and a basal dry mixture, containing casein 41.4 g/L, DL-methionine 0.3 g/L, L-cysteine 0.5 g/L, cellulose 10.0 g/L, xanthan gum 3.0 g/L, corn oil 8.5 g/L, olive oil 28.4 g/L, safflower oil 2.7 g/L, and a standard mineral and vitamin mix for rodent chow (ssniff, Soest, Germany). The control diet consisted of 89.6 g/L maltose dextrin and the basal dry mixture. The mixture was filled up with water to obtain one litre of final solution. Deep-frozen diet was thawed daily and given freshly to the mice. Animals were housed in a 12-hour light-dark-cycle and had free access to the liquid diet, representing the only source of water and nutrition. The treatment protocol was initiated after an accommodation period of 3 days, when animals of all six groups were placed on the liquid control diet. After 5 weeks of treatment, animals were anesthetized by isoflurane inhalation (5% inhalant in room air) and killed by exsanguination via right ventricular puncture. Heart, liver, lung, kidney, spleen and aorta were rapidly excised, transferred to 4 °C Krebs-HEPES-solution (pH 7.35, containing NaCl 99.01 mM, KCl 4.69 mM, CaCl₂ 2.50 mM, MgSO₄ 1.20 mM, NaHCO₃ 25.0 mM, K₂HPO₄ 1.03 mM, Na-HEPES 20.0 mM, D-glucose 11.1 mM), cleared of adhesive tissue and snap-frozen in liquid nitrogen.

Echocardiography. Anaesthesia of mice was induced in a chamber (2–4% isoflurane mixed with 0.2 L/min 100% O₂) and maintained with a face mask (1–2% isoflurane with 0.2 L/min 100% O₂). Animals were kept on a heated table mounted on a rail system (Visual Sonics, Toronto, Canada). Ultrasound was performed with the Vevo 770 System and a 40 MHz mouse transducer (VisualSonics). Heart rate was determined. Body temperature was monitored using a rectal probe and maintained at 37 °C. Left ventricular wall thickness, intraventricular septum thickness, left ventricular end-diastolic and end-systolic volumes and left ventricular shortening fraction were determined. Of note, vital parameters including body temperature and anaesthesia were tightly controlled to minimize iatrogenic effects on the murine cardiac physiology.

Sirius red staining. Hearts were fixed in PFA, embedded in paraffin and sectioned. Paraffin sections were deparaffinized and rehydrated. Nuclei were stained with haematoxylin for 8 min and slides were washed with distilled water (dH₂O). Slides were then completely covered with Picro-Sirius Red solution (Sirius red F3B, Sigma-Aldrich) 0.5 g in 500 mL of saturated aqueous solution of picric acid (1.3%, Sigma-Aldrich) for 60 min. Slides were washed twice in acidified water (5 mL acetic acid in 1 L of dH₂O), dehydrated in successive EtOH baths and mounted in synthetic resin. Images were acquired using an Olympus IX71 microscope, Olympus lenses (plan 20x/0.40/oo/0.17 and plan 40x/0.65/oo/0.17) and Olympus colorView U-TV0.5XC-2 camera (Olympus, Tokyo, Japan) at room temperature. Sections of all study arms were analyzed in parallel with identical imaging parameters.

NOX activity in heart mitochondrial and membrane fractions. Heart mitochondrial and membrane fractions were prepared and measured as previously described^{21,55}. NOX activity (200 μM NADPH) of the membrane suspensions (0.2 mg/ml protein in PBS) was measured by lucigenin (5 μM)-enhanced chemiluminescence (ECL) after incubation with the substrate NADPH (200 μM). Lucigenin-ECL was quantified in a Lumat LB 9507 luminometer (Berthold Technologies, Bad Wildbad, Germany). Results were normalized for protein content and expressed as counts/mg/min after 5 min.

Western Blot analysis and dot blot analysis. Heart, lung, liver, kidney and spleen samples were snap-frozen and homogenized in liquid nitrogen. Pulverized tissue was resuspended in ice-cold homogenization buffer (HB, Tris-HCl 20 mM, sucrose 250 mM, EGTA 3 mM, EDTA 20 mM, aprotinin 10 mg/L, leupeptin 5 mg/L, pepstatin 7 mg/L, PMSF 87 mg/L, cantharidin 0.2 mg/L, triton-X 100 1% (v/v)). Adherent, cultured CMs were collected in ice-cold HB. Pulverized tissue/collected CMs were incubated in HB on ice for 60 min. After centrifugation with 5000 g at 4 °C for 10 min to remove insoluble materials, tissue/CM homogenates were separated by SDS-PAGE (Mini Protean 3, Bio Rad, Hercules, USA) and blotted (Mini-Trans-Blot transfer cell, Bio Rad, Hercules, USA) onto nitrocellulose membranes (Schleicher & Schuell, Dassel, Germany) for Western Blot analysis as described⁵⁶. Briefly, after blocking, immunoblotting was performed with the following antibodies: monoclonal mouse anti α-actinin antibody (1:1000, Cell Signaling, Leiden, Netherlands) as control for loading and transfer and monoclonal mouse anti p67^{phox} antibody (1:1000, Transduction Laboratories, Lexington, USA), mouse monoclonal anti rac1 antibody (1:1000, BD Bioscience, San Jose, USA) and polyclonal goat anti peroxiredoxin 3 antibody (1:340, R&D Systems, Minneapolis, MN, USA). For detection, horseradish peroxidase-labelled secondary antibodies against mouse/rabbit/goat IgG (1:10000, Vector Laboratories, Burlingame, USA) together with ECL reagent (Amersham, Piscataway, USA) were used. The ECL signal was detected with a ChemiLum Imager CsX-1400M (Intas, Göttingen, Germany), while bands were quantified with the Gel-Pro Analyzer software (Media Cybernetics, Bethesda, USA). For dot blot analysis, insoluble materials were removed and tissue homogenates were transferred onto a nitrocellulose membrane with a Minifold I vacuum Dot-Blot system (Schleicher & Schuell, Dassel, Germany) and further processed as described⁵⁷. Briefly, the membrane was washed with PBS and dried at 60 °C for 15 min. For detection of malondialdehyde (MDA)-positive proteins, a polyclonal rabbit antibody against MDA was used (1:2000, Calbiochem, Darmstadt, Germany). Signal detection and quantification was performed as described for Western Blot analysis.

Isolation, purification and culture of adult murine CMs. Adult murine CMs were isolated as described⁵⁸. Briefly, mouse hearts were digested by retrograde perfusion of type 2 collagenase through the

coronary arteries. Live and intact cardiac cells were released by gentle trituration. CMs were purified by repetitive centrifugation due to their characteristic size. After gradual calcium reintroduction, calcium-tolerant cells were plated on mouse laminin-coated dishes in plating media (MEM with Hank's salts, FBS 10%, 2,3 BDM 10 mM, Penicillin 100 U/mL, glutamine 2 mM and ATP 2 mM). After one hour, the plating medium was removed and cells were washed and switched to culture medium (MEM with Hank's salts, BSA 0.1%, penicillin 100 U/mL, glutamine 2 mM, insulin 5 µg/mL, transferrin 5 µg/mL, selenium 5 ng/mL and blebbistatin 25 µM). At this stage, only vital and intact CMs were adhering to the plate. CMs were cultured for 18 h in culture medium conditioned with different doses of EtOH or ACA with/without the NOX inhibitor apocynin (300 µM), compared to culture medium alone at 37 °C and 2% CO₂ in sealed containers to prevent evaporation of EtOH and ACA as described⁵⁸. The incubation time of 18 h was determined empirically as the best compromise of viability of untreated CMs and the most pronounced effect of EtOH/ACA treatment.

Live imaging of CMs and image quantification. In all steps of culture, loading and imaging, cells were kept at 37 °C and 2% CO₂. For staining/assessment of CM (1) mitochondrial abundance/mass, (2) mitochondrial O₂^{•-} production, (3) mitochondrial permeability transition pore (mPTP) opening⁵⁹ and (4) mitochondrial membrane potential ($\Delta\Psi_m$) after exposure to EtOH/ACA, cells were switched to phenol red-free staining medium containing the fluorescent probes: (1) MitoTracker Green FM (100 nM), (2) MitoSOX Red 1 µM, (3) Calcein AM/CoCl₂ 2 µM/1 mmol, (4) tetramethylrhodamin-methyl ester (TMRM⁺) 10 nM (all compounds from Molecular Probes / Thermo Fisher Scientific Inc., Darmstadt, Germany) loaded per protocol (1) 15 min, (2) 10 min, (3) 60 min⁵⁹, (4) 30–45 min at 37 °C, 2% CO₂, in the dark. Cells were imaged in phenol red free culture medium with an automated fluorescence microplate imager with a high-speed laser autofocus and environmental control to minimize phototoxicity due to manual focussing and to obtain unbiased brightness measurements (ImageXpress Micro, Molecular Devices equipped with a Nikon 4 × 0.2 S objective and Semrock filters with the following specifications (Excitation, Emission, Dichroic): TMRM⁺: 589/15 nm, 632/22 nm, >605 nm and MitoSOX Red: 387/11 nm, 607/36 nm, 580 nm). Images were acquired with the standard 1.4 megapixel cooled CCD after illumination by a 300W xenon light source with the MetaXpress software (Molecular Devices). For some experiments, imaging was conducted with an ArrayScanVTI imaging platform (ThermoFisher Scientific Inc. Berkshire, UK). For each probe, fluorescence of individual CM was quantified after background subtraction to account for uneven illumination by particle analysis using FIJI/ImageJ. To exclude debris, only particles larger than 200 pixels (low power field) were counted. For illustration purposes, monochrome images were pseudo-coloured.

Real-time quantitative reverse transcription PCR. The mRNA expression was analyzed by quantitative real-time RT-PCR using a 7900HT Fast Real-Time PCR System (Applied Biosystems, Foster City, CA). Briefly, total RNA from CMs aorta was isolated according to the manufacturer's protocol of the RNeasy mini kit (Qiagen, Hilden, Germany). 50 ng of total RNA was used for real-time RT-PCR analysis with the Power SYBR[®] Green PCR Master Mix (Thermo Fisher Scientific, Karlsruhe, Germany). Primers sequences were obtained from PrimerBank⁶⁰, Sequences: Rac1 forward: GAGACGGAGCTGTTGGTAAAA, reverse: ATAGCCCAGATTCAGTGGTT. CDC42 forward: CCCATCGGAATATGTACCAACTG, reverse: CCAAGAGTGTATGGCTCTCCAC. GABDH forward: AGGTCGGTGTGAACGGATTTG, reverse: TGTAGACCATGTAGTTGAGGTCA. For the remaining targets, 0.1 µg of total RNA was used for RT-PCR analysis with the QuantiTect Probe RT-PCR kit (Qiagen, Hilden, Germany). TaqMan Gene Expression assays (Applied Biosystems, Foster City, CA) were purchased as probe and primer sets. The comparative Ct method was used for relative mRNA quantification (15). Gene expression was normalized to the endogenous control, TBP or GABPH mRNA, and the amount of target gene mRNA expression in each sample was expressed relative to that of control.

Human Biomaterial. We analyzed leftover biomaterial from endomyocardial biopsies obtained from patients who were admitted to our center diagnosed with HF with reduced ejection fraction (HFrEF). Endomyocardial biopsies (EMBs) were taken for diagnostic workup of HF of unknown origin according to current treatment guidelines⁶¹. Written informed consent was obtained from all subjects that leftover biomaterial would be further analysed after pseudonymization. All experiments were in accordance with the Declaration of Helsinki and National Institutes of Health guidelines. All experiments were approved by the Ethics Committee of the University Hospital Mainz.

To assess CM expression of gp91^{phox}, we stained myocardial specimen of 6 males with heart failure with reduced ejection fraction (HFrEF) and a history of excess EtOH consumption (e.g., ≥60g EtOH/d) who had unspecific histologic findings in their routinely examined EMBs, and compared them to matched controls without history of alcohol misuse.

Immunohistochemistry. Slides were deparaffinized in xylene and rehydrated in serial EtOH concentrations. Antigen retrieval was performed in citrate buffer (10 mmol/L sodium citrate, pH 6.0) for 20 min at 99 °C. Slides were blocked with phosphate buffered saline (PBS) with 0.05% Tween-20 and 1% bovine serum albumin (BSA). Primary antibodies were purchased from LifeSpan BioSciences (Seattle, United States) against Nox2/gp91^{phox} (LS-B6247) and from Abcam (Cambridge, United Kingdom) against cardiac Troponin T (ab92546) and CD45 (ab10558). Incubation with primary antibodies was conducted at 4 °C overnight. Secondary antibodies were purchased from Abnova (Heidelberg, Germany) (PAB10815) and from Abcam (ab150116). After three washes in PBS for 5 min, slides were incubated with the secondary antibodies at room temperature in the dark for 1 hour. After three washes in PBS for 5 min each, slides were counterstained with DAPI and mounted. Slides were allowed to cure for 24 hours. Sections were imaged with an Olympus IX73. For quantification, five high power fields were imaged per section. The images were quantified by digital image analysis. To correct for fluorescent background, images were normalized to sections stained with the secondary antibodies only.

Statistical Analysis. Data are expressed as mean \pm SEM. Statistical calculations were performed with GraphPad Prism 5 (GraphPad Software Inc, San Diego, USA). D'Agostino-and-Pearson normality test was first performed, and Kruskal-Wallis test or One-way ANOVA with posthoc Bonferroni multiple comparison test was used as appropriate. Values of $p < 0.05$ were considered significant.

References

- Piano, M. R. Alcoholic cardiomyopathy: incidence, clinical characteristics, and pathophysiology. *Chest* **121**, 1638–1650 (2002).
- Laonigro, I., Correale, M., Di Biase, M. & Altomare, E. Alcohol abuse and heart failure. *European journal of heart failure* **11**, 453–462, doi: 10.1093/eurjhf/hfp037 (2009).
- Di Castelnuovo, A. *et al.* Alcohol dosing and total mortality in men and women: an updated meta-analysis of 34 prospective studies. *Archives of internal medicine* **166**, 2437–2445, doi: 10.1001/archinte.166.22.2437 (2006).
- Skotzko, C. E., Vranceanu, A., Krueger, L. & Freudenberger, R. Alcohol use and congestive heart failure: incidence, importance, and approaches to improved history taking. *Heart failure reviews* **14**, 51–55, doi: 10.1007/s10741-007-9048-8 (2009).
- Knott, C. S., Coombs, N., Stamatakis, E. & Biddulph, J. P. All cause mortality and the case for age specific alcohol consumption guidelines: pooled analyses of up to 10 population based cohorts. *BMJ* **350**, h384, doi: 10.1136/bmj.h384 (2015).
- Aberle, N. S. 2nd & Ren, J. Short-term acetaldehyde exposure depresses ventricular myocyte contraction: role of cytochrome P450 oxidase, xanthine oxidase, and lipid peroxidation. *Alcoholism, clinical and experimental research* **27**, 577–583, doi: 10.1097/01.ALC.0000060522.40447.8E (2003).
- Espinet C., A. J. Ethanol and acetaldehyde levels in rat blood and tissues after an acute ethanol administration. *IRCS Med Sci*, 830–831 (1984).
- Homann, N. *et al.* Alcohol dehydrogenase 1C*1 allele is a genetic marker for alcohol-associated cancer in heavy drinkers. *International journal of cancer. Journal international du cancer* **118**, 1998–2002, doi: 10.1002/ijc.21583 (2006).
- Hintz, K. K. *et al.* Cardiac overexpression of alcohol dehydrogenase exacerbates cardiac contractile dysfunction, lipid peroxidation, and protein damage after chronic ethanol ingestion. *Alcoholism, clinical and experimental research* **27**, 1090–1098, doi: 10.1097/01.ALC.0000075823.73536.DD (2003).
- Guo, R. & Ren, J. Alcohol dehydrogenase accentuates ethanol-induced myocardial dysfunction and mitochondrial damage in mice: role of mitochondrial death pathway. *PLoS One* **5**, e8757, doi: 10.1371/journal.pone.0008757 (2010).
- Duan, J. *et al.* Overexpression of alcohol dehydrogenase exacerbates ethanol-induced contractile defect in cardiac myocytes. *American journal of physiology. Heart and circulatory physiology* **282**, H1216–H1222, doi: 10.1152/ajpheart.00780.2001 (2002).
- Ma, H., Li, J., Gao, F. & Ren, J. Aldehyde dehydrogenase 2 ameliorates acute cardiac toxicity of ethanol: role of protein phosphatase and forkhead transcription factor. *Journal of the American College of Cardiology* **54**, 2187–2196, doi: 10.1016/j.jacc.2009.04.100 (2009).
- Doser, T. A. *et al.* Transgenic overexpression of aldehyde dehydrogenase-2 rescues chronic alcohol intake-induced myocardial hypertrophy and contractile dysfunction. *Circulation* **119**, 1941–1949, doi: 10.1161/CIRCULATIONAHA.108.823799 (2009).
- Chen, C. H. *et al.* Activation of aldehyde dehydrogenase-2 reduces ischemic damage to the heart. *Science* **321**, 1493–1495, doi: 10.1126/science.1158554 (2008).
- Ma, H., Guo, R., Yu, L., Zhang, Y. & Ren, J. Aldehyde dehydrogenase 2 (ALDH2) rescues myocardial ischaemia/reperfusion injury: role of autophagy paradox and toxic aldehyde. *European heart journal* **32**, 1025–1038, doi: 10.1093/eurheartj/ehq253 (2011).
- Agarwal, D. P., Harada, S. & Goedde, H. W. Racial differences in biological sensitivity to ethanol: the role of alcohol dehydrogenase and aldehyde dehydrogenase isozymes. *Alcoholism, clinical and experimental research* **5**, 12–16 (1981).
- Bosron, W. F., Ehrig, T. & Li, T. K. Genetic factors in alcohol metabolism and alcoholism. *Seminars in liver disease* **13**, 126–135, doi: 10.1055/s-2007-1007344 (1993).
- Bell-Parikh, L. C. & Guengerich, F. P. Kinetics of cytochrome P450 2E1-catalyzed oxidation of ethanol to acetic acid via acetaldehyde. *The Journal of biological chemistry* **274**, 23833–23840 (1999).
- Lieber, C. S. Microsomal ethanol-oxidizing system (MEOS): the first 30 years (1968–1998)—a review. *Alcoholism, clinical and experimental research* **23**, 991–1007 (1999).
- Guerri, C., Montoliu, C. & Renau-Piqueras, J. Involvement of free radical mechanism in the toxic effects of alcohol: implications for fetal alcohol syndrome. *Advances in experimental medicine and biology* **366**, 291–305 (1994).
- Daiber, A. *et al.* Measurement of NAD(P)H oxidase-derived superoxide with the luminol analogue L-012. *Free radical biology & medicine* **36**, 101–111, doi: 10.1016/j.freeradbiomed.2003.10.012 (2004).
- Zhang, M., Perino, A., Ghigo, A., Hirsch, E. & Shah, A. M. NADPH oxidases in heart failure: poachers or gamekeepers? *Antioxidants & redox signaling* **18**, 1024–1041, doi: 10.1089/ars.2012.4550 (2013).
- Munzel, T., Gori, T., Keaney, J. F., Jr., Maack, C. & Daiber, A. Pathophysiological role of oxidative stress in systolic and diastolic heart failure and its therapeutic implications. *European heart journal* **36**, 2555–2564, doi: 10.1093/eurheartj/ehv305 (2015).
- Satoh, M. *et al.* Requirement of Rac1 in the development of cardiac hypertrophy. *Proceedings of the National Academy of Sciences of the United States of America* **103**, 7432–7437, doi: 10.1073/pnas.0510444103 (2006).
- Bendall, J. K., Cave, A. C., Heymes, C., Gall, N. & Shah, A. M. Pivotal role of a gp91(phox)-containing NADPH oxidase in angiotensin II-induced cardiac hypertrophy in mice. *Circulation* **105**, 293–296 (2002).
- Bedard, K. & Krause, K. H. The NOX family of ROS-generating NADPH oxidases: physiology and pathophysiology. *Physiological reviews* **87**, 245–313, doi: 10.1152/physrev.00044.2005 (2007).
- Qian, Y. *et al.* Cdc42 regulates arsenic-induced NADPH oxidase activation and cell migration through actin filament reorganization. *J Biol Chem* **280**, 3875–3884, doi: 10.1074/jbc.M403788200 (2005).
- Wang, X. *et al.* Cdc42-dependent activation of NADPH oxidase is involved in ethanol-induced neuronal oxidative stress. *PLoS One* **7**, e38075, doi: 10.1371/journal.pone.0038075 (2012).
- Doughan, A. K., Harrison, D. G. & Dikalov, S. I. Molecular mechanisms of angiotensin II-mediated mitochondrial dysfunction: linking mitochondrial oxidative damage and vascular endothelial dysfunction. *Circulation research* **102**, 488–496, doi: 10.1161/CIRCRESAHA.107.162800 (2008).
- Dikalov, S. I. *et al.* Nox2-induced production of mitochondrial superoxide in angiotensin II-mediated endothelial oxidative stress and hypertension. *Antioxid Redox Signal* **20**, 281–294, doi: 10.1089/ars.2012.4918 (2014).
- Robinson, K. M., Janes, M. S. & Beckman, J. S. The selective detection of mitochondrial superoxide by live cell imaging. *Nat Protoc* **3**, 941–947, doi: 10.1038/nprot.2008.56 (2008).
- Zielonka, J. & Kalyanaraman, B. Hydroethidine- and MitoSOX-derived red fluorescence is not a reliable indicator of intracellular superoxide formation: another inconvenient truth. *Free Radic Biol Med* **48**, 983–1001, doi: 10.1016/j.freeradbiomed.2010.01.028 (2010).
- Kalyanaraman, B. *et al.* Measuring reactive oxygen and nitrogen species with fluorescent probes: challenges and limitations. *Free Radic Biol Med* **52**, 1–6, doi: 10.1016/j.freeradbiomed.2011.09.030 (2012).
- Cox, A. G., Pullar, J. M., Hughes, G., Ledgerwood, E. C. & Hampton, M. B. Oxidation of mitochondrial peroxiredoxin 3 during the initiation of receptor-mediated apoptosis. *Free Radic Biol Med* **44**, 1001–1009, doi: 10.1016/j.freeradbiomed.2007.11.017 (2008).
- Wenzel, P. *et al.* Manganese superoxide dismutase and aldehyde dehydrogenase deficiency increase mitochondrial oxidative stress and aggravate age-dependent vascular dysfunction. *Cardiovasc Res* **80**, 280–289, doi: 10.1093/cvr/cvn182 (2008).

36. Rhee, S. G. *et al.* Intracellular messenger function of hydrogen peroxide and its regulation by peroxiredoxins. *Curr Opin Cell Biol* **17**, 183–189, doi: 10.1016/j.ceb.2005.02.004 (2005).
37. Jones, W. K. A murine model of alcoholic cardiomyopathy: a role for zinc and metallothionein in fibrosis. *The American journal of pathology* **167**, 301–304, doi: 10.1016/S0002-9440(10)62975-6 (2005).
38. Wenzel, P. *et al.* ALDH-2 deficiency increases cardiovascular oxidative stress—evidence for indirect antioxidative properties. *Biochemical and biophysical research communications* **367**, 137–143, doi: 10.1016/j.bbrc.2007.12.089 (2008).
39. Brewer, A. C. *et al.* Nox4 regulates Nrf2 and glutathione redox in cardiomyocytes *in vivo*. *Free radical biology & medicine* **51**, 205–215, doi: 10.1016/j.freeradbiomed.2011.04.022 (2011).
40. Zhang, M. *et al.* NADPH oxidase-4 mediates protection against chronic load-induced stress in mouse hearts by enhancing angiogenesis. *Proceedings of the National Academy of Sciences of the United States of America* **107**, 18121–18126, doi: 10.1073/pnas.1009700107 (2010).
41. Prosser, B. L., Ward, C. W. & Lederer, W. J. X-ROS signaling: rapid mechano-chemo transduction in heart. *Science* **333**, 1440–1445, doi: 10.1126/science.1202768 (2011).
42. Sanchez, G. *et al.* Exercise and tachycardia increase NADPH oxidase and ryanodine receptor-2 activity: possible role in cardioprotection. *Cardiovascular research* **77**, 380–386, doi: 10.1093/cvr/cvm011 (2008).
43. Erickson, J. R. *et al.* A dynamic pathway for calcium-independent activation of CaMKII by methionine oxidation. *Cell* **133**, 462–474, doi: 10.1016/j.cell.2008.02.048 (2008).
44. Wang, M. *et al.* Involvement of NADPH oxidase in age-associated cardiac remodeling. *Journal of molecular and cellular cardiology* **48**, 765–772, doi: 10.1016/j.yjmcc.2010.01.006 (2010).
45. Awad, A. E. *et al.* Tumor necrosis factor induces matrix metalloproteinases in cardiomyocytes and cardiofibroblasts differentially via superoxide production in a PI3Kgamma-dependent manner. *American journal of physiology. Cell physiology* **298**, C679–C692, doi: 10.1152/ajpcell.00351.2009 (2010).
46. Johar, S., Cave, A. C., Narayanapanicker, A., Grieve, D. J. & Shah, A. M. Aldosterone mediates angiotensin II-induced interstitial cardiac fibrosis via a Nox2-containing NADPH oxidase. *FASEB journal: official publication of the Federation of American Societies for Experimental Biology* **20**, 1546–1548, doi: 10.1096/fj.05-4642jfe (2006).
47. Wenzel, P. *et al.* First evidence for a crosstalk between mitochondrial and NADPH oxidase-derived reactive oxygen species in nitroglycerin-triggered vascular dysfunction. *Antioxid Redox Signal* **10**, 1435–1447 (2008).
48. Dikalova, A. E. *et al.* Therapeutic targeting of mitochondrial superoxide in hypertension. *Circulation research* **107**, 106–116, doi: 10.1161/CIRCRESAHA.109.214601 (2010).
49. Eklund, E. A. & Kakar, R. Recruitment of CREB-binding protein by PU.1, IFN-regulatory factor-1, and the IFN consensus sequence-binding protein is necessary for IFN-gamma-induced p67phox and gp91phox expression. *Journal of immunology* **163**, 6095–6105 (1999).
50. Iitsuka, N., Hie, M., Nakanishi, A. & Tsukamoto, I. Ethanol increases osteoclastogenesis associated with the increased expression of RANK, PU.1 and MITF *in vitro* and *in vivo*. *International journal of molecular medicine* **30**, 165–172, doi: 10.3892/ijmm.2012.974 (2012).
51. Oliva, J., Bardag-Gorce, F., Li, J., French, B. A. & French, S. W. S-adenosylmethionine prevents the up regulation of Toll-like receptor (TLR) signaling caused by chronic ethanol feeding in rats. *Experimental and molecular pathology* **90**, 239–243, doi: 10.1016/j.yexmp.2011.01.005 (2011).
52. Kroller-Schon, S. *et al.* Molecular mechanisms of the crosstalk between mitochondria and NADPH oxidase through reactive oxygen species—studies in white blood cells and in animal models. *Antioxidants & redox signaling* **20**, 247–266, doi: 10.1089/ars.2012.4953 (2014).
53. Dikalov, S. I., Li, W., Doughan, A. K., Blanco, R. R. & Zafari, A. M. Mitochondrial reactive oxygen species and calcium uptake regulate activation of phagocytic NADPH oxidase. *American journal of physiology. Regulatory, integrative and comparative physiology* **302**, R1134–R1142, doi: 10.1152/ajpregu.00842.2010 (2012).
54. DeCarli, L. M. & Lieber, C. S. Fatty liver in the rat after prolonged intake of ethanol with a nutritionally adequate new liquid diet. *J Nutr* **91**, 331–336 (1967).
55. Rajagopalan, S. *et al.* Angiotensin II-mediated hypertension in the rat increases vascular superoxide production via membrane NADH/NADPH oxidase activation. Contribution to alterations of vasomotor tone. *J Clin Invest* **97**, 1916–1923 (1996).
56. Wenzel, P. *et al.* Mechanisms underlying recoupling of eNOS by HMG-CoA reductase inhibition in a rat model of streptozotocin-induced diabetes mellitus. *Atherosclerosis* **198**, 65–76, doi: 10.1016/j.atherosclerosis.2007.10.003 (2008).
57. Schuhmacher, S. *et al.* A new class of organic nitrates: investigations on bioactivation, tolerance and cross-tolerance phenomena. *British journal of pharmacology* **158**, 510–520, doi: 10.1111/j.1476-5381.2009.00303.x (2009).
58. O'Connell, T. D., Rodrigo, M. C. & Simpson, P. C. Isolation and culture of adult mouse cardiac myocytes. *Methods Mol Biol* **357**, 271–296, doi: 10.1385/1-59745-214-9:271 (2007).
59. Fraysse, B. *et al.* Ca²⁺ overload and mitochondrial permeability transition pore activation in living delta-sarcoglycan-deficient cardiomyocytes. *Am J Physiol Cell Physiol* **299**, C706–C713, doi: 10.1152/ajpcell.00545.2009 (2010).
60. Spandidos, A., Wang, X., Wang, H. & Seed, B. PrimerBank: a resource of human and mouse PCR primer pairs for gene expression detection and quantification. *Nucleic acids research* **38**, D792–D799, doi: 10.1093/nar/gkp1005 (2010).
61. Cooper, L. T. *et al.* The role of endomyocardial biopsy in the management of cardiovascular disease: a scientific statement from the American Heart Association, the American College of Cardiology, and the European Society of Cardiology Endorsed by the Heart Failure Society of America and the Heart Failure Association of the European Society of Cardiology. *European heart journal* **28**, 3076–3093, doi: 10.1093/eurheartj/ehm456 (2007).

Acknowledgements

We gratefully acknowledge the expert technical assistance of Angelina Hahlbrock, Roland Stauber and Katharina Perius. This work was supported by a grant of the German Foundation for Heart Research F/12/07 to PW. MB, MK, TM and PW received funding from the German Federal Ministry of Education and Research (BMBF 01EO1003) related to this work. HM received funding of the Deutsche Forschungsgemeinschaft (DFG, MO 1695/4-1) related to this work.

Author Contributions

M.B. conceived and coordinated the study, designed, performed and analysed experiments in Figures 1 to 7 and wrote the manuscript. V.G. performed and analysed experiments shown in Figures 3–5. M.O. designed, performed and analysed experiments shown in Figures 1 and 2 and provided technical assistance. E.S. collected patient samples and data. M.K. performed experiments shown in Figures 1, 2 and 6 and helped writing the manuscript. S.K.-S. designed, performed and analysed experiments shown in Figures 1 and 2. S.K. designed, performed and analysed experiments for the revision shown in Figures 4 and 7. T.S. performed experiments shown in Figure 5. H.-P.S. acquired and analysed data in Figure 7. E.S., S.K., H.M., A.D. and T.M. provided

assistance in writing the manuscript. P.W. conceived, coordinated and supervised the study, designed the experiments and wrote the manuscript. All authors reviewed the results and approved the final version of the manuscript.

Additional Information

Supplementary information accompanies this paper at <http://www.nature.com/srep>

Competing financial interests: The authors declare no competing financial interests.

How to cite this article: Brandt, M. *et al.* NOX2 amplifies acetaldehyde-mediated cardiomyocyte mitochondrial dysfunction in alcoholic cardiomyopathy. *Sci. Rep.* **6**, 32554; doi: 10.1038/srep32554 (2016).



This work is licensed under a Creative Commons Attribution 4.0 International License. The images or other third party material in this article are included in the article's Creative Commons license, unless indicated otherwise in the credit line; if the material is not included under the Creative Commons license, users will need to obtain permission from the license holder to reproduce the material. To view a copy of this license, visit <http://creativecommons.org/licenses/by/4.0/>

© The Author(s) 2016